A 28 GHz 8×8 Gapwaveguide Phased Array employing GaN Front-end with 60 dBm EIRP

SUBMISSION DATE / POSTED DATE

08-09-2022 / 12-09-2022

CITATION

Bagherimoghim, Alireza; Bencivenni, Carlo; Gustafsson, Magnus; Alayón Glazunov, Andrés (2022): A 28 GHz 8×8 Gapwaveguide Phased Array employing GaN Front-end with 60 dBm EIRP. TechRxiv. Preprint. https://doi.org/10.36227/techrxiv.21063103.v1

DOI

10.36227/techrxiv.21063103.v1

Communication

A 28 GHz 8×8 Gapwaveguide Phased Array employing GaN Front-end with 60 dBm EIRP

Alireza Bagheri, Carlo Bencivenni, Magnus Gustafsson, and Andrés Alayón Glazunov, *Senior Member, IEEE*

***Abstract*—A high equivalent isotropic radiated power (EIRP) active phased array antenna system has been designed and experimentally verified at the 28 GHz band. The phased array employs Gallium Nitride (GaN) based radio frequency front-ends with 31 dBm output power in transmit mode and 3.5 dB noise figure in receive mode. A fully metallic gapwaveguide technology has been employed in order to achieve an efficient heat dissipation per aperture area of the array as well as low-loss array antenna elements that are easily manufactured. The phased array is realized by sub-arraying an 8×8 slot array antenna with horizontal polarization. The presented antenna system is capable of analog beamforming in the range of $\pm 60^\circ$ in E-plane. The presented high-bandwidth phased array antenna system is a potential candidate for high power and compact size 5G base station antennas for wireless communications requiring high temperature stability at the millimeter-wave bands.**

***Index Terms*—28 GHz, fifth-generation (5G), gapwaveguide based antennas, phased array, mmWave, GaN.**

I. Introduction

THE fifth generation (5G) wireless communications systems aim to provide extremely high data rates at the millimeter-wave (mmWave) frequency bands, e.g., at 24 GHz and above. At these frequencies, the propagation path loss and signal blockage hamper the delivery of multi-Gbps throughput if link margins are not adequately satisfied. This can be overcome by designing transmitters equipped with agile high gain phased arrays and able to deliver high output power at the same time. Currently, a maximum effective isotropic radiated power (EIRP) of approximately 60 dBm is estimated to be required at the base station for outdoor mobile communications systems and for backhauling applications at 28 GHz [1].

To date, several phased arrays have been proposed for 28 GHz 5G applications [2]–[5]. They have been mainly implemented on CMOS and SiGe BiCMOS technologies. These solutions offer great integration flexibility of all circuit functionality, e.g., including phase shifters, variable gain amplifiers (VGA), power amplifiers (PA), and low noise amplifiers (LNA) in a chip [6]. However, the PAs based on these technologies typically deliver an output power at the 1 dB compression point (P1dB) in the range from $9.5 - 16$ dBm [2]–[5], [7]–[9]. This is indeed problematic because in order to achieve a maximum EIRP of at least 60 dBm requires array antennas comprising 256 elements or more [10]–[12].

A technology overcoming output power limitations is the Gallium Nitride (GaN) transistor technology. The GaN technology is a wide band-gap semiconductor technology with high inherent operating voltage. And hence, it can be used to devise PAs able to deliver high output power. The integration of GaN-based PAs and LNAs with phased array antennas has been investigated broadly [10], [13]. The P1dB output powers at the mmWave frequencies have been demonstrated to be typically above 25 dBm. Furthermore, GaN-based LNAs are capable of lower noise figures too, e.g., from 3–4 dB. Therefore, the GaN technology is a good semiconductor technology candidate for mmWaves phased arrays in order to achieve required high EIRP while keeping the size of the phased array antenna smaller [14].

During conversion, a significant amount of DC power is typically lost as dissipated heat. Therefore, in addition to the output power, another important figure of merit of PAs is the power added efficiency (PAE), which is defined as the ratio between the output and input RF power difference to the DC power. Although GaN transistors have typically higher PAE than other technologies, they still achieve only about 20% [10]. Indeed, short wavelengths and the more compact antenna element spacing in mmWave pose challenges regarding the thermal management of high power GaN PAs too. Hence, the PAE needs to be thoroughly considered at the design stage of phased arrays [12]. This has been demonstrated, e.g., for a GaN-based phased array with digital beamforming capabilities, as shown in [12]. Heat pipes were used there to efficiently dissipate the high density heat produced by the PAs for a large antenna comprising 15×24 radiating elements.

In spite of currently published results, and to the best knowledge of the authors, high output power phased array with compact form-factor for 28 GHz 5G applications have not been published yet. Therefore, in this paper, we focus on addressing the challenges for such a compact design regarding antenna element design, beamforming, and handling the heat dissipation of the system integrated with radio frequency front-end (RFFE) transceivers based on the GaN technology. We have designed, manufactured and measured an 8×8 phased array antenna system capable of delivering 61 dBm maximum measured EIRP while consuming 42 W of DC power.

The reminder of the paper is organized as follows. Section II describes the design and integration of the phased array antenna system. Here we first bring the focus on the power budget considerations in the design of the proposed phased array, and later we describe the design details of the array antenna. Section III discusses the verification of the simulations with corresponding measurement results. Conclusions are provided in Section IV.

II. Phased array design

A. Power budget considerations

In order to design a cost-efficient high EIRP phased array at 28 GHz a trade-off among various parameters must be considered. In this section we present our approach for choosing the number and performance of various devices integrated into phased arrays and their impact on the final design. The goal in this approach is threefold, (i) high EIRP, (ii) efficient heat dissipation, and (iii) low cost. The latter is in direct relation with the total number of RF components, e.g., the

Manuscript received April 19, 2005; revised August 26, 2015. This work was partly supported by European Union Horizon 2020 research and innovation program under the Marie Skłodowska-Curie grant agreement No. 766231 WAVECOMBE H2020-MSCA-ITN-2017.

Alireza Bagheri is with the Gapwaves AB, 41263 Gothenburg, Sweden, and also with the Department of Electrical Engineering, University of Twente, 7522 NB Enschede, The Netherlands (email: alireza.bagheri@gapwaves.com).

Carlo Bencivenni, and Magnus Gustafsson are with the Gapwaves AB (email: carlo.bencivenni@gapwaves.com; magnus.gustafsson@gapwaves.com).

Andrés Alayón Glazunov is with the Department of Electrical Engineering, University of Twente, and also with the Department of Electrical Engineering, Chalmers University of Technology, 41296 Gothenburg, Sweden (email: a.alayonglazunov@utwente.nl).

number of antenna elements and associated RFFEs. In this work we focus on one of the most important RF active components, the PAs which in addition to deliver high power need an efficient dissipation of the produced heat for stable operation avoiding failure. The array size and the number RFFEs will add up to the final cost of the phased array and are therefore carefully considered.

We start off by comparing the power budgets for various semiconductor technologies and their potential mix thereof. Table I shows a summary of various parameter designs of active components currently available for the design of phased array antennas at the mmWaves. The focus here is on efficiently achieving the output power and size requirements for a phased array producing a maximum EIRP of 60 dBm employing various PA technologies. The maximum EIRP expressed in dBm has been determined from the following power budget

$$EIRP = G_A + OP_{Tot} - L_F, \tag{1}$$

where

$$G_A = G_{SA} + 10\log N_{FE}, \tag{2}$$

is the total antenna gain in dBi, and

$$OP_{Tot} = OP_{PA} + 10\log N_{FE}, \tag{3}$$

is the total conductive power given in dBm, L_F is the feeding loss given in dB, G_{SA} is the subarray antenna gain, OP_{PA} is the PA output power. The number of subarrays, i.e., RFFEs is denoted by N_{FE}. In this work a subarray is defined as a set of antenna units with linear inter-element spacing of 0.56λ, where λ is the free space wavelength at 29.5 GHz. The subarray antenna gain given in dBi is comuputed as

$$G_{SA} = G_p + 10\log N_p, \tag{4}$$

where N_p is the subarray size, and $G_p = 6$ dBi is the gain of the antenna unit. In linear scale the antenna gain is computed by the well-known formula $G_p\,[linear] = 4\pi A_e/\lambda^2$, which is directly proportional to the effective aperture size $A_e = (0.56\lambda)^2$ of the antenna element. The array spacing with this aperture size ensures a $\pm 60^\circ$ beam scanning capability without grating lobes [15]. The EIRP and the PA output power are computed for the PA's P1dB and 9 dB back off from P1dB (9 dB BO) points. The mmWave wireless communication links use modulation schemes with large dynamic range, such as high-order QAMs and OFDM. This BO ensures that the PA amplifies signals in its linear range without distorting the modulated signal [16].

As shown above, the radiated power depends on the output power of the PA. In turn, the latter is a function of the DC power consumption and the PAE, which are two important design factors for the phased arrays heat dissipation mechanism. Assuming the PA has sufficiently high gain the DC power consumed can be computed in Watts (W) as follows

$$P_{DC} = (OP_{PA} - IP_{PA})/PAE \simeq OP_{PA}/PAE, \tag{5}$$

where OP_{PA} and IP_{PA} are the PA output and input power, respectively.

In order to relate the consumed power to the size of the array antenna we define the power density as

$$\eta_{\text{diss}} = OP_{Tot}/A_{\text{array}}, \tag{6}$$

where the approximate array area can be computed as $A_{\text{array}} \approx N_p N_{FE}(0.56\lambda)^2$, with parameters defined above. η_{diss} is measured in Watts per squared centimeters (W/cm^2). Hence, the power density may be used to evaluate the efficiency of the heat handling mechanism for systems with the same EIRP.

Next we perform a comparative analysis by computing the above enumerated parameters for different hypothetical design configurations employing different semiconductor technologies and their mix.

TABLE I
60 DBM EIRP SOLUTION COMPARISON

	Case		1	2	3	4	5
	PA technology		CMOS	SiGe	SiGe	GaN	GaN
Antenna array	N_p		1	1	4	4	8
	Az. Scan [°]		±60	±60	±60	±60	±60
	El. Scan [°]		±60	±60	±10	±10	-
	G_{SA} [dBi]		6	6	12	12	15
	G_A [dBi]		28.8	25.8	28.8	22.8	24.1
	L_F [dB]		1	1	1	1	1
RF Power	OP_{PA}* [dBm]	P1dB	9.5	16	16	28	28
		9 dB BO	0.5	7	7	19	19
	N_{FE}		192	96	48	12	8
	OP_{Tot} [dBm]	P1dB	32.3	35.8	32.8	38.8	37
		9 dB BO	23.3	26.8	23.8	29.8	28
	EIRP [dBm]	P1dB	60.1	60.6	60.6	60.6	60.1
		9 dB BO	51.1	51.6	51.6	51.6	51.1
DC Power	PA PAE* (9 dB BO)		3%	3%	3%	7%	7%
	P_{DC} / PA (9 dB BO) [W]		0.04	0.17	0.17	$1.13+0.17^\dagger$	$1.13+0.17^\dagger$
	Total P_{DC} (9 dB BO) [W]		7.2	16	8	15.6	10.4
	Array size A_{array}[cm^2]		69	35	69	17.3	23
	Power density η_{diss} [W/cm^2]		0.1	0.46	0.12	0.9	0.45

* Values are taken from [5], [8], [17]
† In this case, each RF chain is assumed to have both SiGe and GaN PAs.

We consider five different cases which results are summarized in Table I. As mentioned above, CMOS and SiGe PAs offer great flexibility and therefore we consider them in Cases 1, 2 and 3, where we put emphasis on achieving maximum beam scanning range, low P_{DC} or both. However, the use of GaN PAs, considered in Cases 4 and 5, results in compact phased arrays employing fewer RFFEs. The primary use of the GaN technology for mmWaves phased array antennas are in the realization of PAs and LNAs. Meanwhile, other functional blocks such as phase shifters and variable gain amplifiers can be equally realized on CMOS and SiGe BiCMOS technologies, which support the functionalities. Therefore, a hybrid module combining CMOS or SiGe beamformers and GaN-based RFFEs is an excellent solution for meeting both the high output power and the low cost requirements in the design of 5G phased array antennas, which is considered in cases 4 and 5.

Cases 1 and 2 in Table I illustrate the power budget of phased arrays with subarray size $N_p = 1$, employing CMOS and SiGe PAs, respectively. Given G_{SA}, OP_{PA} and L_F, the number of front-ends N_{FE} is computed from (1) in order to achieve EIRPs equal to 60 dBm and 51 dBm, at P1dB and at 9 dB BO, respectively. The computed EIRPs have been slightly increased to obtain realistic array sizes. It is worthwhile to note that due to subarray size $N_p = 1$, both cases 1 and 2 are able to cover the full $\pm 60^\circ$ scanning range in both azimuth and elevation planes. The total P_{DC} of each case is the sum of the consumed DC power of all PAs. Therefore, cases 1 and 2 with about 3% PAE at 9 dB BO will consume 7.2 and 16 W, respectively. The average power densities η_{diss} for Cases 1 and 2 are 0.1 and 0.46 W/cm^2, respectively. Hence, by considering equal PAE for both cases, SiGe will produce more heat. Meanwhile, N_{FE} is reduced by half for Case 2 resulting in less RF components needed.

Case 3 shows the power budget of a phased array employing a SiGe-based PA with a subarray size of $N_p = 4$ elements in the azimuth direction. Comparing cases 2 and 3 can give an indication of advantages and disadvantages of subarraying. While DC power consumption OP_{Tot} and the number of subarrays N_{FE} are decreased to half due to subarraying, the total size of the array is doubled. In other words, for a fixed EIRP, the subarraying increases the array gain G_A,

while decreasing OP_{Tot}. Therefore, the power density is decreased in Case 3, which requires a simpler heat dissipation solution. It is worthwhile to note that employing a subarray size of 4 elements in the vertical direction, the elevation scanning range becomes limited to $\pm 10^{\circ}$, as the closest spacing of the subarray elements is at least 2.2λ. Although, in this case subarraying reduces the steering capability, some deployment scenarios, e.g., low-rise urban, suburban, and rural environments, have limited user spread in the vertical direction, therefore a reduced scanning range is still acceptable [18].

Cases 4 and 5 represent GaN-based solutions with a high OP1dB PA power output and subarray sizes with 4 and 8 elements, in the elevation direction. The PA's high output power aids in shrinking the array's size, even when radiating elements are subarrayed. N_{FE} is decreased significantly in both cases. Currently, there are no off-the-shelf GaN-based beamformer integrated circuits (BFICs). Hence, a SiGe-based BFIC is added in the beamforming power budget calculation. To maintain the steering capability of $\pm 60^{\circ}$ in one plane, subarraying of radiating elements in the other plane is required, because the spacing between RFFEs in the steering plane should not exceed the limit 0.56λ. While employing larger subarraying size in case 5, the scanning range becomes almost negligible in elevation plane, it has half the power density compared to Case 4.

Research on the GaN PAs at mmWave frequencies has been mostly restricted to developing their functional characteristics, such as, gain, output power, efficiency, etc. Our paper examines their application to deliver high power in the context of analog beamforming phased array antennas. The remainder of this section will be devoted to the design of a phased array satisfying the requirements of the power budget computations listed in Case 5.

B. Front-end design

Fig. 1 shows that four dual channel RFFEs and two BFICs are used in the PCB design. The RFFEs are based on 150 nm GaN on SiC process from Qorvo. This device operates from $26-30$ GHz, and contains an LNA, a transmit/receive switch, and a PA. The receive path including the LNA plus switch, provides 17 dB of gain and a typical noise figure of 3.5 dB. The transmit path including the PA plus switch, provides 27 dB of small signal gain with high linearity at $OP_{PA} = 22$ dBm average output power, while supporting peak power of 31 dBm and P1dB of 28 dBm [19]. Each BFIC has four bidirectional channels and each channel has a transmit and a receive chain. These contain a high resolution phase shifter and VGA to perform analog beamforming. The VGA gain control in the TX and RX chains are supporting a maximum of 25 dB and 30.5 dB, respectively [20]. The use of two stages of amplifiers helps to have high output power in receive mode and a good margin for the input signal level in transmit mode.

C. Antenna element and transition design

The gapwaveguide (GW) technology is a low-loss waveguide and packaging technology for mmWaves operation that also offers a good thermal conductivity performance [21], [22], and it can be realized fully metallic. Therefore, the GW technology is a good candidate for phased arrays with high power dissipation and compact size [14]. A center-fed vertical subarray of 8 vertical slots is used as the antenna element, as shown in Fig. 2(a). The initial designs of the subarray element and the array are reported in [23] and therefore an in-depth presentation of the design has been omitted here. Two symmetric ridge GW lines are used to excite the slots. They are fed from the center of subarray. The ridge and pin sizes are designed to cover the target frequency band, following design rules in [21]. The width and height of the subarray are 0.56λ and 5λ, respectively.

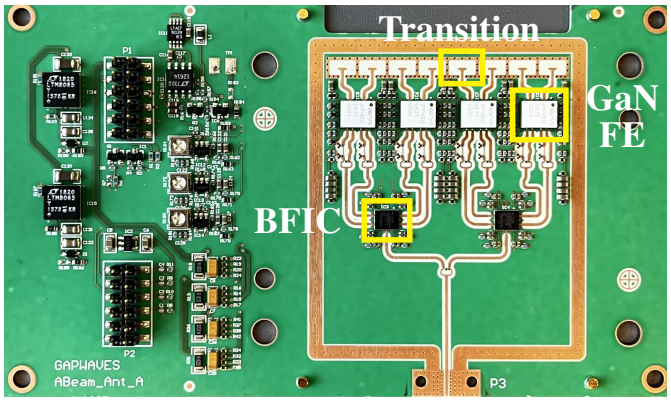

Fig. 1. Photograph of PCB employing four dual channel GaN RFFEs, which are connected to 8 antenna feeds.

In order to maximize the power transfer to the radiating element from the GaN-based RFFE, a through-substrate probe transition from microstrip to ridge GW has been used. The vertical, compact and contactless transition is a practical solution for phased arrays as it leaves space below the antenna for PCB routing and active components [24]. The designed transition simulation and measurement results with a two-layer 10 mil Rogers RO4350 substrate are reported in [14]. The presented results show a 0.2 dB insertion loss and -20 dB input matching (S_{11}) from $26.5-29.5$ GHz.

Fig. 2(a) shows the subarray and transition cascaded to each other. A bed of pins is placed over the microstrip probe to provide a back short. A ridge GW line connects the transition to the feeding point of the subarray at its center. The subarray is simulated with CST Microwave Studio's time domain solver. The embedded input

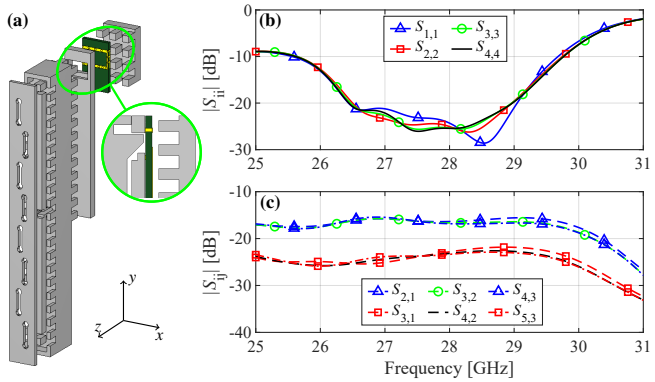

Fig. 2. (a) Exploded view of the subarray. yz-plane cross section of microstrip line transition to ridge gapwaveguide line is highlighted. Embedded element simulation results for (b) input matching and (c) mutual coupling.

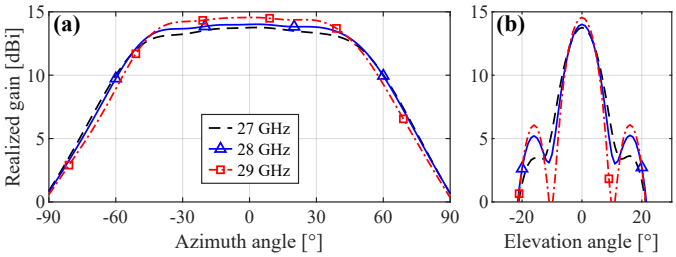

Fig. 3. Embedded radiation pattern of the central subarray in (a) azimuth (E-plane) and (b) elevation (H-plane).

matching of half of the elements are shown in Fig. 2(b). It shows that the bandwidth at $S_{11} < -10$ dB is from $26.5 - 29.5$ GHz. The embedded mutual coupling between adjacent and every other elements are shown in Fig. 2(c), which remains under -16 dB. The embedded radiation pattern of the subarray in the center of the array is shown in Fig. 3. The average of the embedded realized gains, computed over all subarrays, increases from 13.8 to 15 dBi over the frequency band of interest. This is expected because the size of aperture in terms of wavelength increases with frequency. This is in line with the design goal set in the Table I, where the subarray gain and the feeding loss were considered to be equal to 15 and 2 dB, respectively. The radiation pattern is narrow in the elevation plane (H-plane) due to subarraying, while a wide beamwidth in azimuth (E-plane) is achieved. The realized gain variation within $\pm 60^\circ$ has a minimum and maximum of 3.5 and 6 dB, respectively. At 29.5 GHz gain variation is the largest. This can be attributed to the pattern becoming slightly more directive at higher frequencies. The cross polarization ratio is lower than -35 dB in the azimuth plane.

TABLE II
COMPARISON WITH STATE OF THE ART PHASED ARRAYS AT 28 GHZ

Ref.	**This work**	[29]	[14]	[12]
PA Tech.	**150nm GaN**	SiGe BiCMOS	SiGe BiCMOS	150nm GaN
Ant. Tech.	**Gapwaveguide**	Stacked patch	Gapwaveguide	n/a
OP_{PA} P_{sat} [dBm]	**31**	-	17	33
OP_{PA} P1dB [dBm]	**28**	16	-	-
Beamfoming Architecture	**Analog**	Analog	Analog	Digital
Array Size	$\mathbf{8 \times 8}$	8×8	8×8	15×24
Subarray Size	**8**	1	4	15
N_{FE}	**8**	64	16	24
EIRP [dBm]	**58***	55*	51**	75
Scan Range (Az./El.) [°]	$\pm\mathbf{60}/-$	$\pm 50/\pm 40$	$\pm 45/\pm 10$	$\pm 60/-$
Tx Total P_{DC} [W]	**42***	21.8*	13***	n/a
Tx Total P_{DC} / N_{FE} [W]	**5.25***	0.34*	0.812***	n/a

*At P1dB. **At Psat. ***At 8 dB BO.

III. CALIBRATION AND MEASUREMENTS

Fig. 4 shows the manufactured prototype of the phased array antenna proposed in this paper. The structure consists of five layers, where all the metal layers have been manufactured by Aluminum milling. The PCB is placed between the shield layer and the cooling layer, which is an efficient way to stabilize the temperature of RF active components on the PCB. This solution was proposed previously in [14], [25]. In this arrangement, the GaN components dissipate their heat directly into shield layer, and through PCB to cooling layer. The shield layer has a bed of pins used for transition back-short, and also to suppresses unwanted cavity modes. The cooling layer hosts the openings for microstrip transition, and also acts as a conductive plane over the ridge gap waveguide.

The phased array's performance is characterized and calibrated in transmit mode. All measurement process is performed in the farfield using a vector network analyzer and a standard gain horn antenna. To achieve the intended performance, active phased arrays must be calibrated. It is usually done by adjusting the relative phase between channels. Although the design produced has been realized symmetrically in all parts, there will be unavoidable variance between channels due to, e.g., edge effects, manufacturing, assembly, and component differences, particularly due to varying BFICs' performance. Inconsistency in the phases of a phased array channels results in beams with lower gain and higher side lobe levels as compared to the magnitudes [26]. In this work, channel phase calibration has been performed as presented in [27]; details are omitted here for the sake of compactness. This process offers the minimum requirement for the hardware, has a simple process and suits best for arrays with small number of elements [28]. The calibration was performed only at 28 GHz broadside, and applied to all frequencies and steering angles. The symmetry in the design allowed a simplification of the calibration procedure and reduced calibration measurement time. The results presented in the following are calibrated.

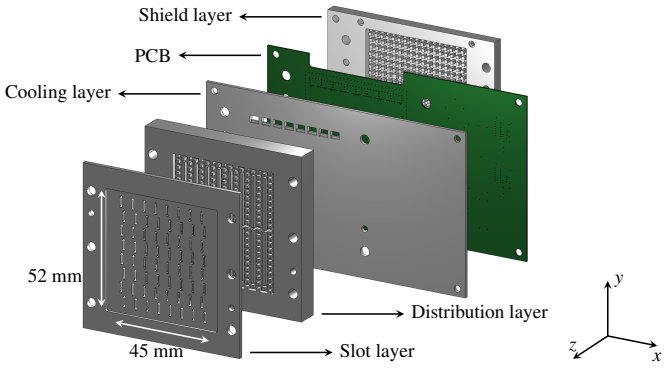

Fig. 4. Exploded view of the phased array antenna's stack-up.

Fig. 5 shows the measured normalized radiation pattern in azimuth plane at 28 GHz only, because it corresponds to the center frequency of the band. The main beam was measured at steering angles -30°, 0°, and 30° as shown in subplots Fig. 5 (a), (b) and (c), respectively. The measured side lobe levels are < -10 dB for all radiation patterns, and the 3-dB beamwidth equals to 12° and 14° in the in broadside and the $\pm 30^\circ$ directions, respectively. As can be seen from Fig. 5, the measurement results agree well with the simulations. The calibrated measurement EIRP beam patterns at three different frequencies are shown in Fig. 6. The phased array beams span a field-of-view within the $\pm 60^\circ$ range in the azimuth plane (E-plane). This is in line with value specified in Table I. As can be seen from Fig. 6, the EIRP increases with frequency, because the antenna gain of the sub-array element increases with frequency. Meanwhile, the PA's gain decreases slightly with frequency, but the antenna gain increase dominates. The maximum EIRP of far steering angles are lower than in the broadside. This is because the effective aperture area is reduced when the phased array's beam points to angles other than broadside as expected. It has already been shown in the embedded radiation pattern of the center subarray, Fig. 3(a).

The EIRP in the broadside direction versus input signal power is shown in Fig. 7(a) at three frequencies. The EIRP at P1dB is equal to 57, 57.5 and 60 dBm at 27, 28, and 29 GHz, respectively. The maximum measured EIRP at these frequencies is 59.5, 61, and 62.5 dBm, respectively. It should be noted that even though every factor that could reduce systematic error was taken into account, the measurement results are estimated to have an uncertainty of ± 0.5 dB. This uncertainty is due to the combined result of the angular misalignment of the antennas, the ICs' temperature drift, and the noise introduced by the measurement equipment. In comparison to the values provided in Case 5 of Table I, the design achieves its EIRP goal at 29 GHz. This difference can have multiple sources, e.g., the differences between the PAs' performance, the PAs going into compression at lower input power, and higher loss in the feeding lines, transitions, and antenna elements. The direction of maximum EIRP of the scanned beams in the E-plane are shown in Fig. 8. The 21 separate beams are measured over the whole operational frequency

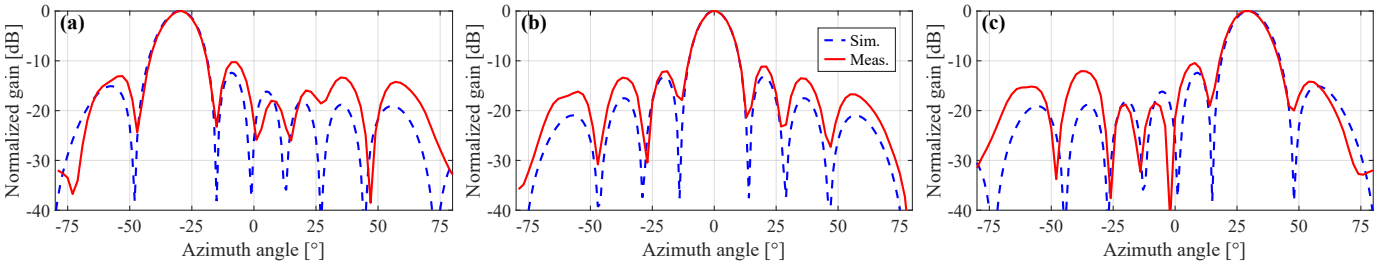

Fig. 5. Measured patterns in azimuth plane (E-plane) at (a) $-30°$, (b) $0°$, and (c) $30°$. All patterns are normalized to their maximum value.

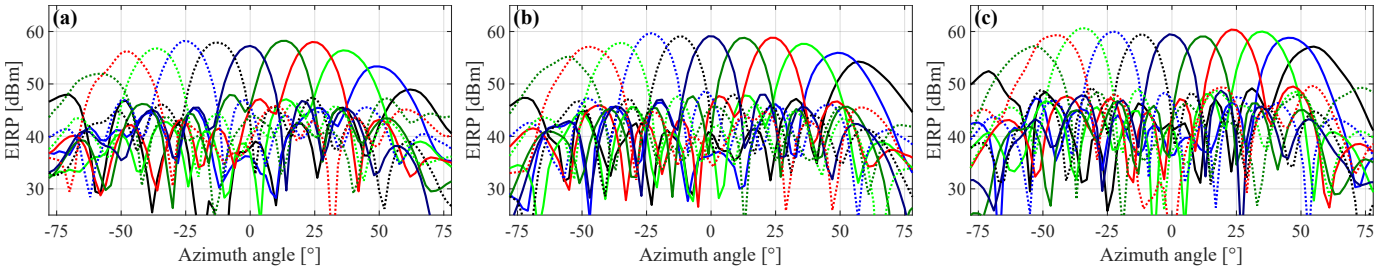

Fig. 6. Measured beams in terms of EIRP with -3 dBm input power, in azimuth plane at (a) 27, (b) 28, and (c) 29 GHz.

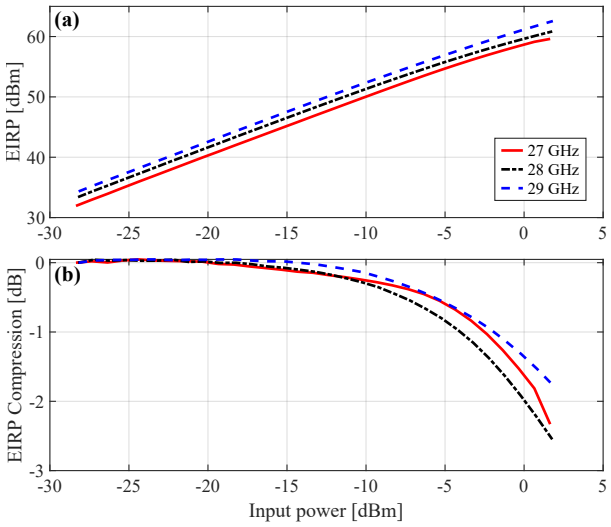

Fig. 7. (a) EIRP measurement, and (b) EIRP compression of broadside angle beam versus RF input power at three frequencies.

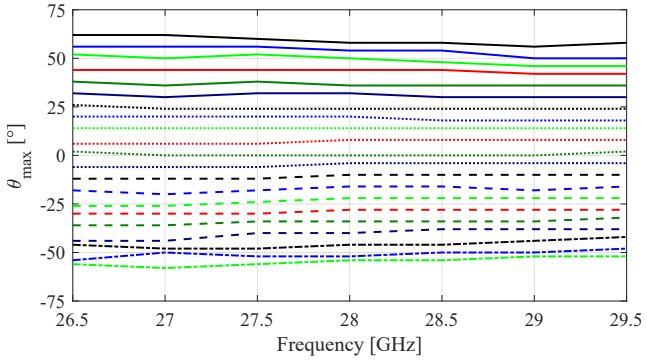

Fig. 8. Measured direction of maximum EIRP (θ_{max}) of the beams in E-plane.

band. All the beams are measured after calibrating the phased array at broadside angle at 28 GHz. While the beams cover $\pm 60°$ angular range at 28 GHz, the range is larger at lower frequencies and smaller at higher frequencies. This is due to beam squint effect while steering the beams over a wide frequency band [15].

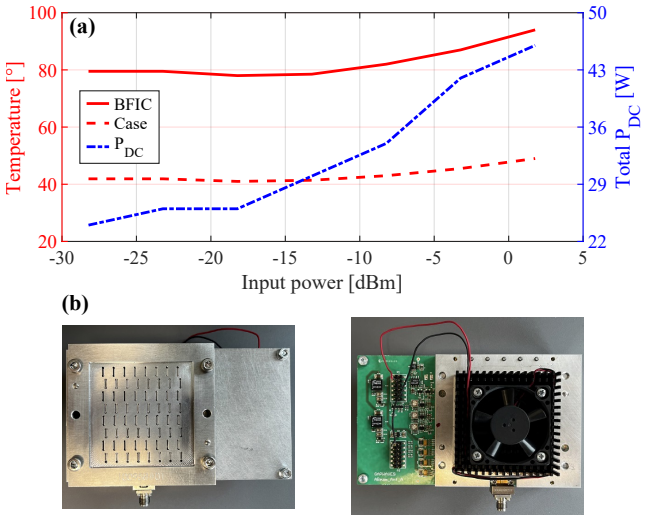

Fig. 9. (a) Temperature readout of the BFIC and the phased array's case, and total DC power consumption versus RF input power in TX mode. (b) Front and back view of the manufactured phased array prototype.

The measured temperatures of BFIC and the case of the antenna versus RF input power are shown in Fig. 9(a). The case temperature was read both in front and back of the phased array, as shown in 9(b). The GaN-based RFFE and SiGe-based BFIC have the maximum operating temperature of around 100°C. The figure shows that the phased array can support high power while having a temperature that all circuitry can handle. Because GaN-based RFFE has no integrated thermometer, its temperature cannot be measured directly. 9(a) also displays the phased array's total DC power consumption. It represents the total power consumed by the PA and other components. The system as a whole consumes approximately 42 W of DC power at P1dB and 30 W at 9 dB BO. According to the estimates presented in Table I, the PAs deliver 10.4 W at 9 dB BO. The difference between

measurement and estimation values has two origins. Firstly, the measured value considers the whole phased array system, including PAs. And secondly, the PAE of the practical PA might be lower than what has been assumed in Table I.

Table II summarizes the performance of the phased array antenna system presented here and compares it with state of the art high EIRP phased arrays at 28 GHz. Compared with published 8×8 arrays, the proposed design in this paper shows higher EIRP while using less active components. Achieving higher EIRP is equivalent with higher power consumption.

IV. Conclusion

The design and experimental verification of the performance of a compact high-EIRP phased array based on GaN high power amplifiers and gapwaveguide antenna technology has been presented. The phased array is capable of delivering 60.5 dBm EIRP at the saturation regime. It covers a scanning range of $\pm 60^{\circ}$ in azimuth plane, and supports the frequency range of 26.5 to 29.5 GHz. The use of fully metallic antenna structure helps to stabilize the antenna temperature due to an efficient heat power dissipation mechanism, while delivering high EIRP with a relatively small array size of 8×8 elements as compared to previous designs. It is expected that this design has a potential application as a highly efficient and low-cost base station antenna system for 5G wireless communications systems.

References

[1] P. M. Asbeck, N. Rostomyan, M. Özen, B. Rabet, and J. A. Jayamon, "Power amplifiers for mm-wave 5G applications: Technology comparisons and CMOS-SOI demonstration circuits," *IEEE Transactions on Microwave Theory and Techniques*, vol. 67, no. 7, pp. 3099–3109, 2019.

[2] B. Sadhu, Y. Tousi, J. Hallin, S. Sahl, S. K. Reynolds, Ö. Renström, K. Sjögren, O. Haapalahti, N. Mazor, B. Bokinge, *et al.*, "A 28-ghz 32-element trx phased-array ic with concurrent dual-polarized operation and orthogonal phase and gain control for 5g communications," *IEEE Journal of Solid-State Circuits*, vol. 52, no. 12, pp. 3373–3391, 2017.

[3] J. Dunworth, B.-H. Ku, Y.-C. Ou, D. Lu, P. Mouat, A. Homayoun, K. Chakraborty, A. Arnett, G. Liu, T. Segoria, *et al.*, "28GHz phased array transceiver in 28nm bulk CMOS for 5G prototype user equipment and base stations," in *2018 IEEE/MTT-S International Microwave Symposium-IMS*, pp. 1330–1333, IEEE, 2018.

[4] K. Kibaroglu, M. Sayginer, T. Phelps, and G. M. Rebeiz, "A 64-element 28-GHz phased-array transceiver with 52-dBm EIRP and 8–12-Gb/s 5G link at 300 meters without any calibration," *IEEE Transactions on Microwave Theory and Techniques*, vol. 66, no. 12, pp. 5796–5811, 2018.

[5] H.-T. Kim, B.-S. Park, S.-S. Song, T.-S. Moon, S.-H. Kim, J.-M. Kim, J.-Y. Chang, and Y.-C. Ho, "A 28-ghz cmos direct conversion transceiver with packaged 2×4 antenna array for 5g cellular system," *IEEE Journal of Solid-State Circuits*, vol. 53, no. 5, pp. 1245–1259, 2018.

[6] D. Zhao, P. Gu, J. Zhong, N. Peng, M. Yang, Y. Yi, J. Zhang, P. He, Y. Chai, Z. Chen, *et al.*, "Millimeter-wave integrated phased arrays," *IEEE Transactions on Circuits and Systems I: Regular Papers*, vol. 68, no. 10, pp. 3977–3990, 2021.

[7] J. Pang, R. Wu, Y. Wang, M. Dome, H. Kato, H. Huang, A. T. Narayanan, H. Liu, B. Liu, T. Nakamura, *et al.*, "A 28-ghz cmos phased-array transceiver based on lo phase-shifting architecture with gain invariant phase tuning for 5g new radio," *IEEE Journal of Solid-State Circuits*, vol. 54, no. 5, pp. 1228–1242, 2019.

[8] B. Ustundag, K. Kibaroglu, M. Sayginer, and G. M. Rebeiz, "A wideband high-power multi-standard 23–31 GHz 2×2 quad beamformer chip in SiGe with $>$15 dBm OP1dB per channel," in *2018 IEEE Radio Frequency Integrated Circuits Symposium (RFIC)*, pp. 60–63, IEEE, 2018.

[9] K. Kibaroglu, M. Sayginer, A. Nafe, and G. M. Rebeiz, "A dual-polarized dual-beam 28 GHz beamformer chip demonstrating a 24 Gbps 64-QAM 2×2 MIMO link," in *2018 IEEE Radio Frequency Integrated Circuits Symposium (RFIC)*, pp. 64–67, IEEE, 2018.

[10] A. Inoue, "Millimeter-Wave GaN Devices for 5G: Massive MIMO Antenna Arrays for Sub-6-GHz and mm-Wave Bandwidth," *IEEE Microwave Magazine*, vol. 22, no. 5, pp. 100–110, 2021.

[11] Y. Yin, Z. Zhang, T. Kanar, S. Zihir, and G. M. Rebeiz, "A 24-29.5 ghz 256-element 5g phased-array with 65.5 dbm peak eirp and 256-qam modulation," in *2020 IEEE/MTT-S International Microwave Symposium (IMS)*, pp. 687–690, IEEE, 2020.

[12] T. Kuwabara, N. Tawa, Y. Tone, and T. Kaneko, "A 28 GHz 480 elements digital AAS using GaN HEMT amplifiers with 68 dBm EIRP for 5G long-range base station applications," in *2017 IEEE Compound Semiconductor Integrated Circuit Symposium (CSICS)*, pp. 1–4, IEEE, 2017.

[13] L. Belostotski and S. Jagtap, "Down with noise: an introduction to a low-noise amplifier survey," *IEEE Solid-State Circuits Magazine*, vol. 12, no. 2, pp. 23–29, 2020.

[14] C. Bencivenni, T. Emanuelsson, and M. Gustafsson, "Gapwaves Platform Integrates 5G mmWave Arrays," *Microwave Journal*, vol. 62, no. 2, 2019.

[15] R. J. Mailloux, *Phased array antenna handbook*. Artech house, 2017.

[16] H. Wang, P. M. Asbeck, and C. Fager, "Millimeter-wave power amplifier integrated circuits for high dynamic range signals," *IEEE Journal of Microwaves*, vol. 1, no. 1, pp. 299–316, 2021.

[17] QPF4001, *26-30 GHz 1 Watt GaN Front End Module*. Qorvo.

[18] P. von Butovitsch, D. Astely, C. Friberg, A. Furuskär, B. Göransson, B. Hogan, J. Karlsson, and E. Larsson, "Advanced antenna systems for 5G networks," *Ericsson White Paper*, 2018.

[19] QPF4002, *26-30 GHz 1 Watt GaN Dual Channel Front End Module*. Qorvo.

[20] MMW9002KC, *26.5-29.5 GHz 4-Channel Analog Beamforming Integrated Circuit*. NXP Semiconductors.

[21] P.-S. Kildal, E. Alfonso, A. Valero-Nogueira, and E. Rajo-Iglesias, "Local metamaterial-based waveguides in gaps between parallel metal plates," *IEEE Antennas and wireless propagation letters*, vol. 8, pp. 84–87, 2008.

[22] A. U. Zaman, M. Alexanderson, T. Vukusic, and P.-S. Kildal, "Gap waveguide pmc packaging for improved isolation of circuit components in high-frequency microwave modules," *IEEE Transactions on Components, Packaging and Manufacturing Technology*, vol. 4, no. 1, pp. 16–25, 2013.

[23] A. Bagheri, C. Bencivenni, and A. A. Glazunov, "mmWave Array Antenna based on Gap Waveguide Technology for 5G Applications," in *2019 International Conference on Electromagnetics in Advanced Applications (ICEAA)*, pp. 0492–0494, IEEE, 2019.

[24] A. Bagheri, H. Karlsson, C. Bencivenni, A. Haddadi, T. Emanuelsson, and A. A. Glazunov, "Microstrip to ridge gap waveguide transition for 28 ghz steerable slot array antennas," in *2020 14th European Conference on Antennas and Propagation (EuCAP)*, pp. 1–4, IEEE, 2020.

[25] C. Bencivenni, M. Gustafsson, A. Haddadi, A. U. Zaman, and T. Emanuelsson, "5g mmwave beam steering antenna development and testing," in *2019 13th European Conference on Antennas and Propagation (EuCAP)*, pp. 1–4, IEEE, 2019.

[26] A. Bagheri, H. Karlsson, C. Bencivenni, M. Gustafsson, T. Emanuelsson, M. Hasselblad, and A. A. Glazunov, "A 16×16 45° slant-polarized gap-waveguide phased array with 65 dbm eirp at 28 ghz," *IEEE Transactions on Antennas and Propagation*, [To be published].

[27] T. Takahashi, Y. Konishi, S. Makino, H. Ohmine, and H. Nakaguro, "Fast measurement technique for phased array calibration," *IEEE Transactions on Antennas and Propagation*, vol. 56, no. 7, pp. 1888–1899, 2008.

[28] G. Magalhães, J. León, and M. de Menezes, "A novel calibration method for phased-array radar based on element-wise time offsetting and multi-element phase toggle," in *2019 IEEE Radar Conference (RadarConf)*, pp. 1–6, IEEE, 2019.

[29] Y. Yin, B. Ustundag, K. Kibaroglu, M. Sayginer, and G. M. Rebeiz, "Wideband 23.5–29.5-GHz phased arrays for multistandard 5G applications and carrier aggregation," *IEEE Transactions on Microwave Theory and Techniques*, vol. 69, no. 1, pp. 235–247, 2020.